Millimeter Wave Radar System for Standoff Detection Applications: Motion Compensation and 3D Imaging Capabilities

Galia Ghazi, Fernando Quivira, Jose A. Martinez and Carey M. Rappaport

Work supported by Gordon - CENSSIS, ALERT, and Northeastern University, Boston, MA 02115 (ghazi.g@husky.neu.edu)

October 18, 2010

Abstract

In this poster we present a new motion compensation algorithm used for improving the SAR images measured by a standoff detection radar system. The radar system works in a multiple bistatic configuration. The receiver is moved across a 1.85 m aperture and the transmitter is always located at the center of the aperture. The motion compensation algorithm has been applied to data collected on a real Frequency Modulated Continuous Wave (FMCW) radar system. The algorithm corrects for the relative movement existing between the target and the radar system by using a corner cube as a reference. This poster also presents the imaging capabilities of a millimeter wave radar system consisting of an array of receivers located on a two dimensional aperture. The latter configuration is able to produce 3D images, which ultimately improves the probability of detection of potential hazards.

Introduction

We use the SAR image processing of the measurements from a FMCW radar. The Radar has the following parameters: center frequency=94.2GHz, bandwidth=4GHz and pulse burst duration= 83.36μs. This system has both monostatic and bistatic receiving antennas. The bistatic antenna is moved across a linear aperture of 1.85 m length. The velocity of the receiving antenna is not constant across the linear aperture producing distortions in the final image. The acceleration, velocity and position of the receiving antenna can be estimated by using a corner cube as a reference point. The estimation algorithm is based on a non linear optimization algorithm, which is explained in the next section.

Algorithm

Fig. 1(a) shows the basic configuration of the measurement. It consists of a human person, who is the target under test, one metallic array, located at the left hand side of person, and a corner cube at the right hand side of the person. The position of the bistatic antenna during its motion is depicted in Fig. 1(b). So the equations (1) to (3) can be derived for the position of the antenna in different parts of its motion. Knowing the position of the antenna we can define the measured distance of the corner cube as in equation (4). So we optimized the unknown parameters in these equations via the measured distance of the corner cube.

$$x(t) = \frac{1}{2}\, a_1 t^2 \qquad (t < t_1) \quad (1)$$

$$x(t) = \; a_1\, t_1\, (t - t_1) + \frac{1}{2} a_1\, t_1^2 \qquad (t_1 < t < t_2) \quad (2)$$

$$x(t) = \frac{1}{2}\, a_2\, (t - t_2)^2 + a_1\, t_1\, (t - t_2) + a_1\, t_1\, t_2 + \frac{1}{2}\, a_1\, t_1^2 \qquad (t > t_2) \quad (3)$$

$$distance = \sqrt{(x0 + x1)^2 + y0^2} + \sqrt{(x0 + x(t))^2 + y0^2} \quad (4)$$

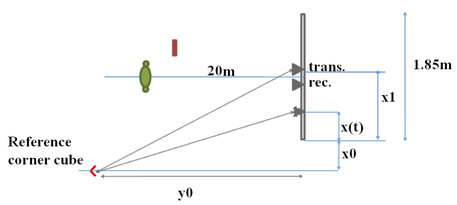

(a)

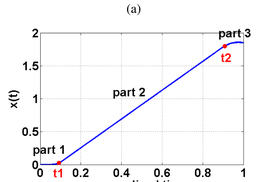

(b)

Figure 1: (a) bistatic and monostatic configuration. (b) Bistatic antenna position.

Results

- Using the new optimized parameters we can process the measured data to examine the images. Figs. 2(a) and 2(b) present the image of the corner cube after and before applying the aforementioned algorithm. In Fig. 2(b) we have considered the static transmitting and receiving antennas to be located at the center of the aperture, and discarded all records collected outside the constant velocity region (part 2 of Fig. 1(b)). The same comparison for the images of the array is illustrated in Figs. 3(a) and 3(b).

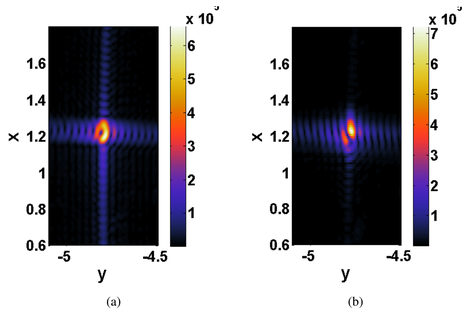

(a) (b)

Figure 2: image of the corner cube (a) with optimization algorithm. (b) approximate image considering only the records with constant velocity for antenna.

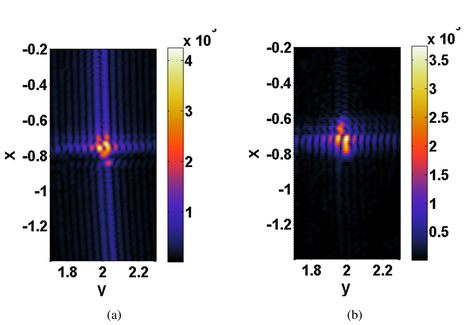

(a) (b)

Figure 3: image of the array (a) with optimization algorithm. (b) approximate image considering only the records with constant velocity for antenna.

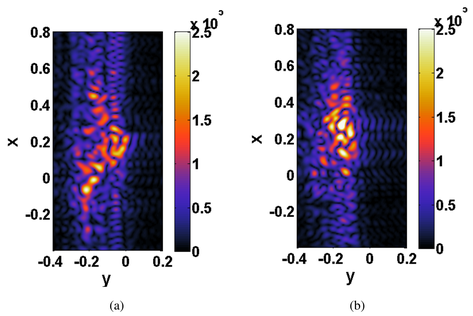

(a) (b)

Figure 4: image of the body (a) without any threat. (b) with metallic pipes on the chest.

- The images of the body without any threat and with the threat using this algorithm are depicted in Figs. 4(a) and 4(b). The threat consists of four metallic pipes on the chest of the person. For the threat case (4(b)) there is a higher intensity of the field level, which is more concentrated on the front surface of the body.

3D imaging simulation

The SAR processing is also used to simulate the 3D images of the targets using a planar array of static antennas.

- Fig. 5 presents the baseline configuration used in this work. It consists of a rectangular antenna array located at $R = 20$m from the target. The transmitting array is made of a single transmitter located at the center of the antenna. The receiver array consists of 26 line receivers uniformly distributed along a 0.7m $\hat{z}$-aperture. Each line receiver is comprised of 46 single receivers uniformly distributed along a 1.85m $\hat{x}$-aperture.

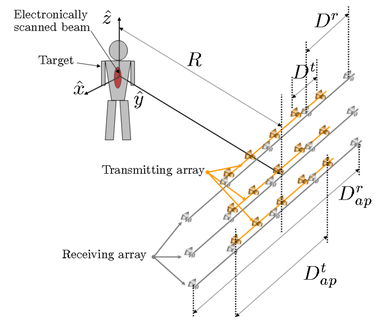

Figure 5: Antenna array and target configuration

- The study tested the image reconstruction algorithm against 2 different geometries: male body and male body with metallic cylindrical pipes on the chest (Fig. 7).
- The simulation treated the centroid of every triangular patch in the body mesh model as an individual point source. The intensity of each individual point source was proportional to the area of the corresponding triangular patch.
- In the case shown in Fig. 6(b), the 5 cylindrical metallic pipes have a radius $r = 0.01$m and a height $h = 0.2$ m.
- Figs. 7(a) and 7(b) show the reconstructed reflectivity of the observation space. Figs. 7(a) shows the reconstructed image for the body without metallic pipes. Figs. 7(b) shows the reconstructed images for the body with cylindrical metallic pipes on the chest. The difference between these two sceneraios is better displayed in Fig. 7(c) when we choose a higher threshold for the equiamplitude reflectivity..

Conclusion

In this poster we have described a new motion compensation algorithm, which has been used to improve the quality of SAR images generated in standoff detection scenarios. We have also presented the imaging capabilities of a system composed of a two dimensional aperture of receiving antennas. The two dimensional array is able to generate 3D images, which substantially improves the probability of threat detection.

References

[1] Martinez-Lorenzo J. A., Rappaport C. M.. SAR imaging of suicide bombers wearing concealed dielectric structures. Accepted to be published, HST 2010 — IEEE International Conference on Technologies for Homeland Security, Walthan, MA, Nov. 2010.

[2] Curlander J. C., McDonough R. N., Synthetic Aperture Radar: Systems and Signal Processing, John Wiley Sons, Inc., USA, 1991.

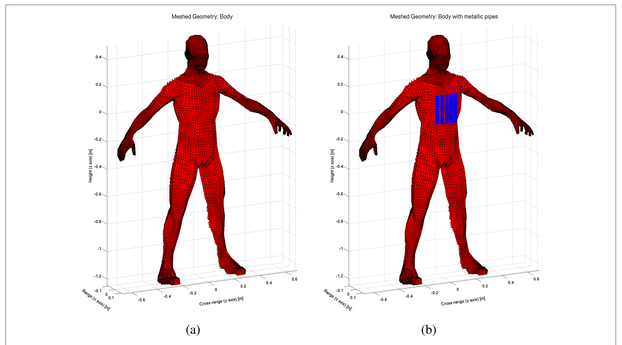

(a) (b)

Figure 6: Target geometry used in the simulation: (a) body without metallic pipes, and (b) body with metallic pipes

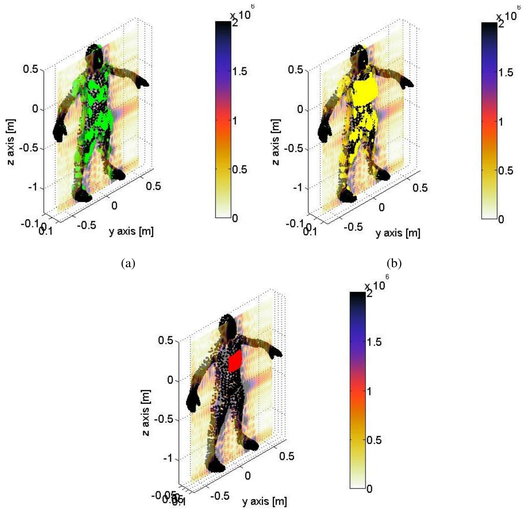

(a) (b)

(c)

Figure 7: Image reconstruction: (a) Reflectivity and isocontours of body without metallic pipes (b) reflectivity and isocontours of body with 5 cylindrical metallic pipes (c)reflectivity and isocontours of body with 5 cylindrical metallic pipes with higher threshold

[3] Carrara W. G., Goodman R. S., Majewski R. M., Spotlight Synthetic Aperture Radar: Signal Processing Algorithms, Artech House, Inc., USA, 1995.

[4] Chen V. C., Ling H., Time-Frequency Transforms for Radar Imaging and System Analysis, Artech House, Inc., USA, 2002.

Acknoledgements

This material is based upon work supported by Gordon-CenSSIS Center for Subsurface Sensing and Imaging Systems (Award Number EEC-9986821) and the U.S. Department of Homeland Security (Award Number 2008-ST-061-ED0001). The views and conclusions contained in this document are those of the authors and should not be interpreted as necessarily representing the official policies, either expressed or implied of the U.S. Department of Homeland Security.